

# The variation of ENSO characteristics associated with atmospheric parameter perturbations in a coupled model

Thomas Toniazzo · Matthew Collins ·  
Josephine Brown

Received: 20 December 2006 / Accepted: 29 August 2007 / Published online: 11 October 2007  
© Springer-Verlag 2007

**Abstract** We analyse the differences in the properties of the El Niño Southern Oscillation (ENSO) in a set of 17 coupled integrations with the flux-adjusted, 19-level HadCM3 model with perturbed atmospheric parameters. Within this ensemble, the standard deviation of the NINO3.4 deseasonalised SSTs ranges from 0.6 to 1.3 K. The systematic changes in the properties of the ENSO with increasing amplitude confirm that ENSO in HadCM3 is prevalently a surface (or SST) mode. The tropical-Pacific SST variability in the ensemble of coupled integrations correlates positively with the SST variability in the corresponding ensemble of atmosphere models coupled with a static mixed-layer ocean (“slab” models) perturbed with the same changes in atmospheric parameters. Comparison with the respective coupled ENSO-neutral climatologies and with the slab-model climatologies indicates low-cloud cover to be an important controlling factor of the strength of the ENSO within the ensemble. Our analysis suggests that, in the HadCM3 model, increased SST variability localised in the south-east tropical Pacific, not originating from ENSO and associated with increased amounts of tropical stratocumulus cloud, causes increased ENSO

variability via an atmospheric bridge mechanism. The relationship with cloud cover also results in a negative correlation between the ENSO activity and the model’s climate sensitivity to doubling CO<sub>2</sub>.

## 1 Introduction

While recent coupled atmosphere–ocean global circulation models (AOGCMs) have improved in terms of their representation of the present-day characteristics of El Niño Southern Oscillation (ENSO) and associated remote climate impacts (e.g. AchutaRao and Sperber 2006), uncertainties in models continue to limit their usefulness for seasonal climate predictions and for the assessment of the impact of climate change on ENSO and ENSO teleconnections (van Oldeborgh et al. 2005; Guilyardi 2006; Merryfield 2006).

In particular, while some AOGCMs appear to match the observed ENSO phenomenology better than others (van Oldeborgh et al. 2005), the representation of the climate mean state and its seasonal cycle in the tropical Pacific, and of the present-day ENSO and its teleconnections, is imperfect (e.g. Capotondi et al. 2005; Joseph and Nigam 2006) in all current AOGCMs. Moreover, the properties of the simulated ENSO are sensitive not only to the climate mean-state and to the annual cycle (Guilyardi 2006; Toniazzo 2006), but also to the formulation of the numerical model, and in particular of the atmospheric component (Guilyardi et al. 2004). The question then arises of how uncertainties in models affect their ability to provide a reliable tool for prediction.

In seasonal forecasting, it is possible to assess skill over a number of verification cycles and make corrections

---

T. Toniazzo (✉)  
The Walker Institute, Department of Meteorology,  
University of Reading, Reading RG6 6BB, UK  
e-mail: t.toniazzo@reading.ac.uk

M. Collins  
Hadley Centre for Climate Prediction and Research,  
Met Office, Exeter, UK

J. Brown  
School of Geography and Environmental Science,  
Monash University, Clayton, Victoria, Australia

for model uncertainties in probabilistic predictions (Coelho et al. 2006). In climate change prediction, no such verification is possible. This has led to attempts to quantify uncertainties in climate predictions by examining the uncertain components of the models in a systematic way, for example by perturbing parameters which control key physical feedbacks in the system (Murphy et al. 2004). Here, we adopt this framework and analyse the properties of the simulated ENSO in a set of 17 versions of the HadCM3 coupled ocean–atmosphere GCM which differ from one another by the value of some key parameters used in the physical parametrisation of sub-grid-scale processes. These affect aspects of the atmospheric physics such as cloud radiative forcing and convection (Collins et al. 2006a, 2006b). The ocean component is the same in each member of this ensemble and for each member a flux adjustment field is applied, obtained from a spin-up stage with a relaxation-type Haney forcing of the SSTs and the SSSs towards a reference climatology (Johns et al. 1997). The ensemble can thus be considered, to some degree, as a sample of AOGCMs having an identical ocean component, with very similar upper-ocean climatologies that are maintained by the flux adjustment fields, and atmospheric components that differ, by construction, in their physical properties. This makes it a suitable tool for the study not only of the potential spread in the properties of the ENSO (Brown et al. 2006), but also of the relationships between the characteristics of the atmospheric mean state and those of the ENSO, as represented in the HadCM3 AOGCM.

By using an ensemble of flux-adjusted integrations of one model with controlled perturbations to some aspects of the atmospheric physics, our study is complementary to multi-model analysis work (e.g. Philip and van Oldenborgh 2006) where compensating effects of concurrent changes in the mean climatology of different equilibrium solutions occur. Nevertheless, the wide spectrum of ENSO properties found within our perturbed-physics ensemble parallels the similar spread in the multi-model ensemble. Such behaviour of coupled GCMs is important for two reasons. First, it suggests that there may be an inconsistency between modelling techniques with reduced-complexity models, where the atmospheric response to SST anomalies is kept fixed or parametrised crudely, and calculations with complex AOGCM. Second, it implies that we still cannot rule out the possibility, as the mean properties of the atmosphere are affected by climate change, of significant consequences for the ENSO, which we are not yet in a position to quantify. The present paper is meant to contribute to our understanding of how current model uncertainties reflect on uncertainties in the range of possible behaviours of the ENSO, and on the mechanisms that control that spread.

## 2 The perturbed physics ensemble

The ensemble we examine is described in detail in Collins et al. (2006a, 2006b); a subset of this ensemble has been used to simulate palaeoclimate conditions for the mid-Holocene in Brown et al. (2007). It comprises 17 versions of HadCM3 (Gordon et al. 2000; Collins et al. 2001), one with the standard parameter settings and 16 versions in which 29 of the atmosphere component parameters are simultaneously perturbed (see Table 1 of Collins et al. 2006a, 2006b). Simultaneous parameter perturbations allow for interactions between uncertainties in different physical processes. The perturbations lead to a range of transient climate response, the 20-year average temperature change at the time of CO<sub>2</sub> doubling in an experiment in which CO<sub>2</sub> is increased at a rate of 1% per year, of 1.5–2.6. This is similar to the range seen in the AOGCMs submitted for comparison as part of the Fourth Assessment Report (“AR4”) of the Inter-governmental Panel on Climate Change (<http://www.ipcc-data.org>). Thus a plausible range of feedbacks associated with global-mean changes are sampled.

Perturbing parameters leads to imbalances in top-of-the-atmosphere (“TOA”) radiation and hence we employ flux-adjustments to all model versions (Johns et al. 1997). Each ensemble member is run for many centuries with a seasonally-varying Haney forcing of both salinity and temperature. When global stability is achieved, the Haney forcing term is averaged to produce a seasonally varying but fixed flux of freshwater and heat which is applied at the ocean surface. During the Haney phase, variability is suppressed due to the relatively strong restoration of the surface climatology. However, and as we shall see later, when the flux-adjustment terms (a separate surface flux for each perturbed-physics version) are applied, the model does produce a rich spectrum of interannual variability.

Flux adjustment has the benefit of correcting many of the regional SST biases seen in the HadCM3 and thus does improve the ability to simulate ENSO teleconnections more accurately. However, flux adjustment also has the potential to influence, for example, the coupled feedbacks that determine the mean location of the convective and of the subsidence areas, and the strength and structure of the trade-winds system, and those that are determinant for the properties of the ENSO. Spencer et al. (2007) discuss the impacts of using various forms of flux adjustment in HadCM3 on ENSO variability. They find that, in the case of globally-applied, local flux adjustments (as used here), the correction of the SST field reveals a bias in the atmospheric component of the model which leads to increased easterlies in central-east Pacific, steepening the thermocline in that region. This tends to inhibit the formation of large ENSO events associated with sub-surface

propagation of anomalies in heat content. When flux adjustments are applied only close to the equator, easterlies are weakened and large events are permitted more often. Model errors, however, remain influential even when surface biases are corrected, and their impact needs to be further understood and quantified.

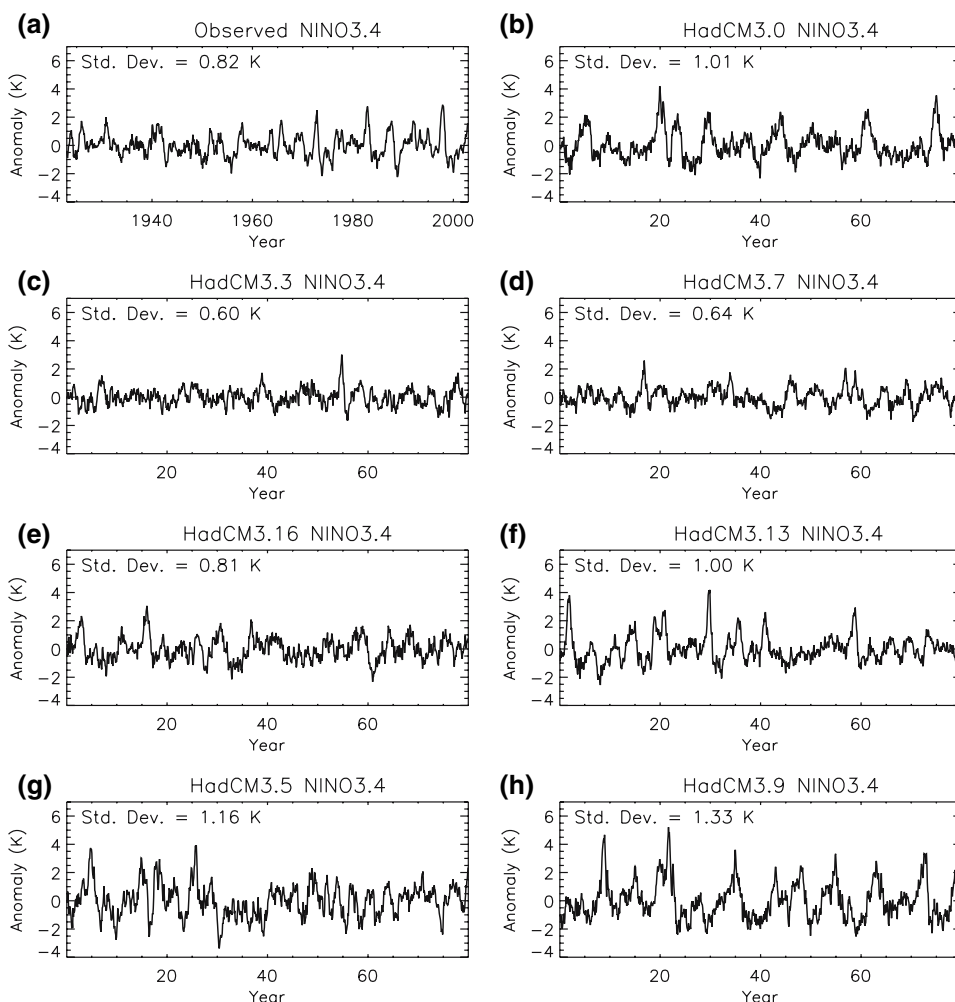
Thus ENSO in HadCM3 (and presumably other coupled AOGCMs) is sensitive to the introduction of flux adjustments and to the precise way those adjustments are applied, consistent with the expectation that ENSO is sensitive to variations in mean climate conditions. In this study, the flux adjustments for each member are calculated in precisely the same way and are, in fact, very similar spatially. The leading-order difference between the flux-adjustments fields for each member is in the global-mean value which prevents model drift. Thus the carefully-controlled nature of experimental set-up provides a suitable framework for examining the impact of atmospheric model parameter perturbations on ENSO properties in this particular model set-up.

### 3 Characteristics of ensemble ENSO variability

The basic characteristics of the ENSO variability across the perturbed physics ensemble are revealed by examining time series of NINO3.4 anomalies (Fig. 1). Due to the spatial differences in the ENSO SST anomaly pattern (see later), use of the NINO3 index to characterise the ENSO properties would be less appropriate as it is not representative of the model ENSO-like variability especially for members with weaker variability. The NINO3.4 region spans an area including the centre of action of all ensemble members and correlates well with the respective leading-EOF time series

Perhaps surprisingly, within the ensemble different (“perturbed”) values of model parameters controlling aspects of the atmospheric physics result in a wide range of ENSO amplitudes and frequencies. Such variations are consistent with the findings of Guilyardi et al. (2004) who showed the importance of atmospheric processes in determining ENSO characteristics. The representative ensemble

**Fig. 1** Time series of monthly-mean NINO3.4 SST anomalies (computed with respect to monthly annual climatologies) from **a** SST observations (HadISST dataset, Rayner et al. 2003), **b** the flux-adjusted HadCM3 control experiment with standard parameter settings and **c–h** from a few of the 16 ensemble members with perturbed atmosphere parameters. A total of 80 years of each experiment are shown



members shown in Fig. 1 have a NINO3.4 variability that, compared with the observed value of 0.81, ranges from very weak [e.g. members HadCM3.3 and HadCM3.7 using the notation of Collins et al. (2006a, 2006b)] to very strong (e.g. member HadCM3.9), including near-observed values (e.g. member HadCM3.13).

There are also variations in the main period of ENSO across the ensemble and these are correlated with the variations in ENSO amplitude (Fig. 2). In general, model versions which have high amplitude ENSO variability have a lower frequency oscillation than those with smaller amplitude. Similarly, the longitudinal location of the maximum in SST variability is also correlated with the amplitude (Fig. 2) and period. ENSO variability of larger amplitude tends to be located further east.

### 3.1 Atmospheric ENSO anomalies

The main characteristics of the ENSO “mode” in the ensemble as a whole are revealed by examining the zero-lag spatial correlations of SST, precipitation and zonal wind fields with the NINO3.4 index for each member. Figure 3 shows the average over the whole ensemble. The SST anomalies are maximum in the central/eastern Pacific, in contrast to the version of HadCM3 without flux-adjustment in which anomalies extend erroneously into the West Pacific warm-pool region (presumably associated with the mean cold bias in that region). Precipitation anomalies occur to the West of the maximum SST anomalies, consistent with the eastward migration of the warm pool.

Coincident with these precipitation anomalies are the anomalies in zonal wind stress and associated shift in low-level convergence. The simulated ENSO anomalies are in reasonable agreement with observed ones (not shown), but the model shows a lack of variability in the East Pacific, and narrower meridional range.

In Fig. 4 we illustrate the variation of the anomalies associated with this mode of variability within the ensemble, which is concomitant with the variations in the amplitude, the mean period and the location of maximum variability shown in Fig. 2. In order to draw out the leading-order differences, we identify five members with the strongest ENSO and the five members with the weakest ENSO and examine the difference between the composite modes for each case. To obtain a uniform normalisation, the characteristic anomalies are computed as the time-covariance of the monthly anomalies of the quantity of interest (e.g. precipitation) with the NINO3.4 index, divided by the variance of the NINO3.4 index. For the rest of this article we shall refer to such quantities as “regressions”. Figure 4 shows that the eastward displacement of the SST pattern with stronger ENSO (highlighted in Fig. 2 above) is accompanied by an eastward shift in anomalous low-level winds and precipitation from convective rainfall.

We tested whether the sensitivity of the wind response to localised equatorial SST anomalies, i.e. the slope of the linear regression of surface zonal wind anomalies over the Equator with respect to SST anomalies in various areas along the Equator, is related with the ENSO strength within the ensemble. The result is that the relation is weak, and negative in sign (a behaviour already noted in Toniazzo

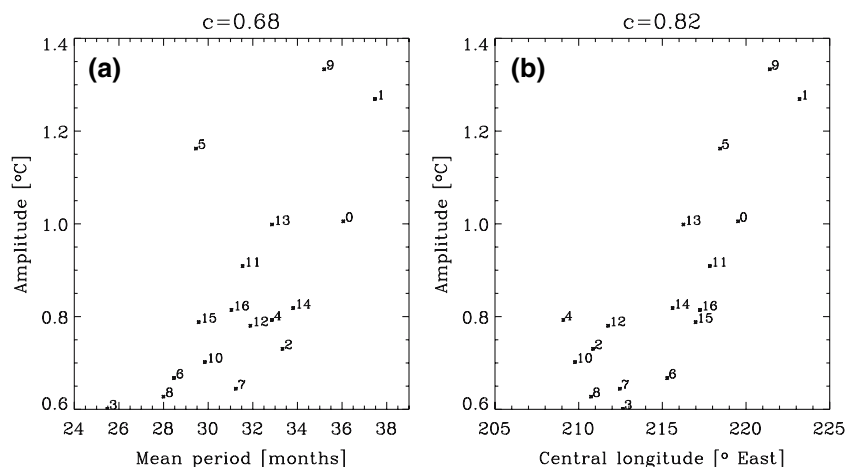


**Fig. 2** *Left panel* ENSO period, measured as the weighted mean period of the deseasonalised, smoothed NINO3.4 index, using the Fourier power distribution as weights, for members of the perturbed physics ensemble against the corresponding ENSO amplitude, measured by the standard deviation (*SD*) of NINO3.4. *Right panel* The longitudinal position of the maximum interannual SST

variability, located by computing the leading EOF of interannual SST anomalies in the tropical Pacific region, against ENSO amplitude. The numbers indicate version numbers following Collins et al. (2006a, 2006b) with the standard version indicated by a zero. The first 80 years of each ensemble simulation were used to compute the measures

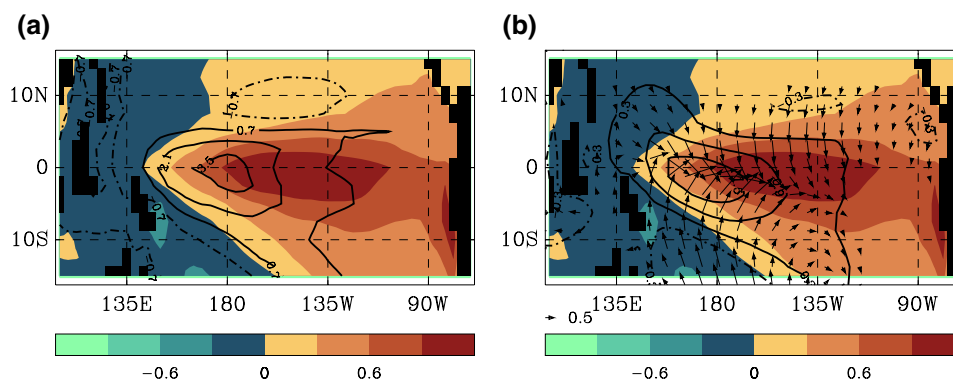


**Fig. 3** Ensemble-average fields of the regressions of SSTs, precipitation and 10-m winds onto the NINO3.4 index. The regressions are computed for each member separately, at each grid-point for each field, before averaging across the ensemble. **a** Colours show SST anomaly correlations (blue for negative values, contour interval  $0.3^{\circ}\text{C}^{\circ}\text{C}^{-1}$ ) and black contours show precipitation anomaly correlations (solid lines for positive correlations, dot-dashed for negative

values, in intervals of  $1.4\text{ mm day}^{-1}\text{ }^{\circ}\text{C}^{-1}$ ). **b** Colours as in **a**, contours show the cross-correlation with the zonal component of the 10-m wind anomaly (contour interval is  $0.6\text{ m s}^{-1}\text{ }^{\circ}\text{C}^{-1}$ ) and arrows show the cross-correlation with the 10-m wind anomaly vectors (scale  $0.5\text{ m s}^{-1}\text{ }^{\circ}\text{C}^{-1}$  at the bottom left of the panel—arrows are not plotted for magnitudes less than half of this value)

2006), implying that differences in the wind response by themselves cannot account for the spread in ENSO. We also note that there is no relation across the ensemble between the amplitude of the ENSO (or its period) and the strength or the timing of its seasonal locking. The NINO3.4 variability peaks in December or January in all members, with two exceptions (members 2 and 5) where the November variance is slightly larger than the December variance.

### 3.2 Oceanic ENSO anomalies

The temperature and density structure of the upper ocean (0–300 m) near the Equator is very similar in all members.

This might to some extent be expected, as the ocean model component is not perturbed, and for each ensemble member temperature and salinity flux adjustment fields are applied such as to achieve a monthly ocean-surface climatology which is close to that observed.

For ENSO-related anomalies, there are no significant cross-ensemble correlations between the strength of the ENSO in each member and the correlation between anomalous SST tendencies created by subsurface temperature anomalies and the monthly increments of the SST (i.e. the difference in the SST between one month and the following) along the Equator (e.g. in the NINO3.4 region). A stronger thermocline feedback is expected to result in an increasing tendency for eastward propagation or stationarity of the SST anomalies along the Equator (Jin and Neelin

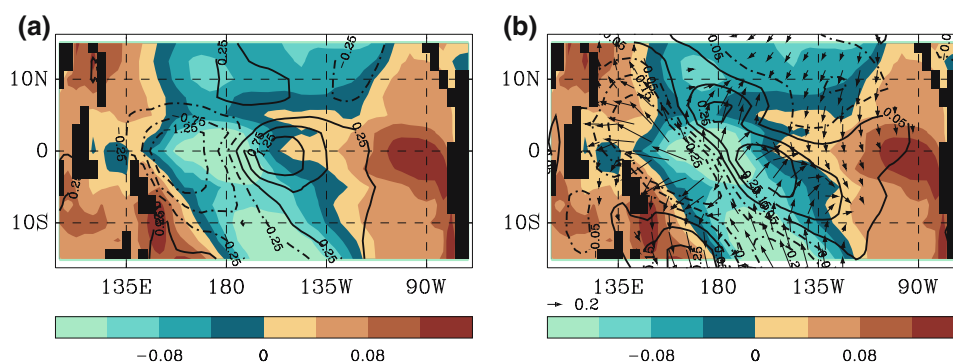


**Fig. 4** Similar to Fig. 3 but showing the differences between the average regressions of anomalies onto NINO3.4 of members 0, 1, 5, 9, 11, 13 (mean NINO3.4 SD  $1.11^{\circ}\text{C}$ ) and of members 2, 3, 6, 7, 8 and 10 (mean  $0.66^{\circ}\text{C}$ ). **a** Colours represent regression differences for SSTs (blue for negative values, contour interval  $0.04^{\circ}\text{C}^{\circ}\text{C}^{-1}$ ), black contours indicate regression differences for precipitation. **b** Colours

as in **a**, contours indicate regression differences for the zonal component of the 10-m wind (intervals of  $0.1\text{ m s}^{-1}\text{ }^{\circ}\text{C}^{-1}$ ) and arrows show the regression differences for the 10-m wind anomaly vectors (scale  $0.2\text{ m s}^{-1}\text{ }^{\circ}\text{C}^{-1}$  on the bottom left of the panel—arrows are not plotted for magnitudes less than half of this value)



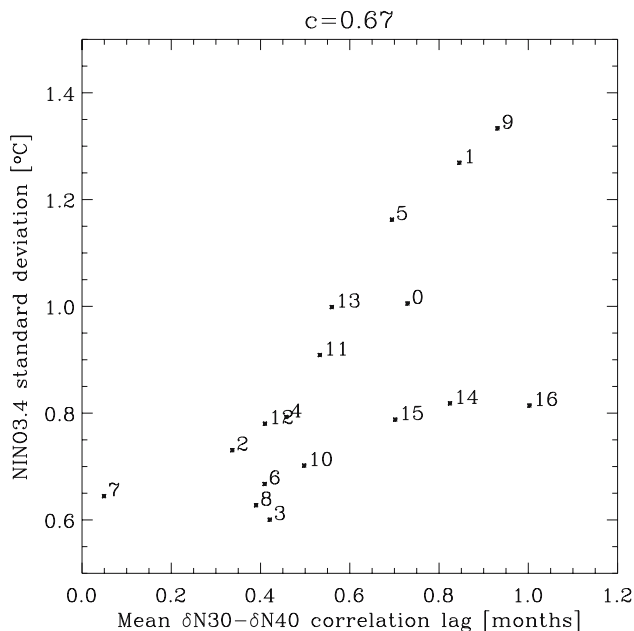


**Fig. 5** The relationship between ENSO strength and the propagation characteristics of equatorial SST anomalies across the ensemble. The *x*-axis indicates values for the lag-correlation-weighted mean lag (in months) between monthly increments of the monthly-mean NINO4 index and of the monthly-mean NINO3 index. Positive lags are for  $\delta$ NINO4 lagging  $\delta$ NINO3, indicating predominant westward propagation

1993), which is not found here. Figure 5 uses a diagnostics that Toniazzo (2006) has shown to reflect the main propagation characteristics of ENSO anomalies in HadCM3. Positive lags of the monthly NINO4 increments,  $\delta$ NINO4, with respect to monthly NINO3 increments,  $\delta$ NINO3, imply a westward propagation of the surface anomaly. When the lag-correlation-weighted mean lag of  $\delta$ NINO4 with respect to  $\delta$ NINO3 is positive, westward propagation is thus diagnosed to be prevalent. Ensemble members with a stronger ENSO tend to display a more marked westward propagation of the SST anomalies, consistently with a surface (or “SST”) mode mainly dependent on wind-driven zonal and vertical advective anomalies of the climatological ocean-temperature field (Jin and Neelin 1993).

The small impact of thermocline anomalies on the strength of the ENSO is consistent with other studies of the HadCM3 model (Toniazzo 2005, 2006; Spencer et al. 2007) that indicate that the simulated ENSO is dominated by the advection-dependent surface (or “SST”) mode (Jin and Neelin 1993). In flux-adjusted integrations, this tendency becomes more severe (Spencer et al. 2007) and the pattern of wind response to SST anomalies affects the implied magnitude of the SST tendency anomalies simply through the climatological zonal gradient in the thermocline depth. This in turn affects the strength of the

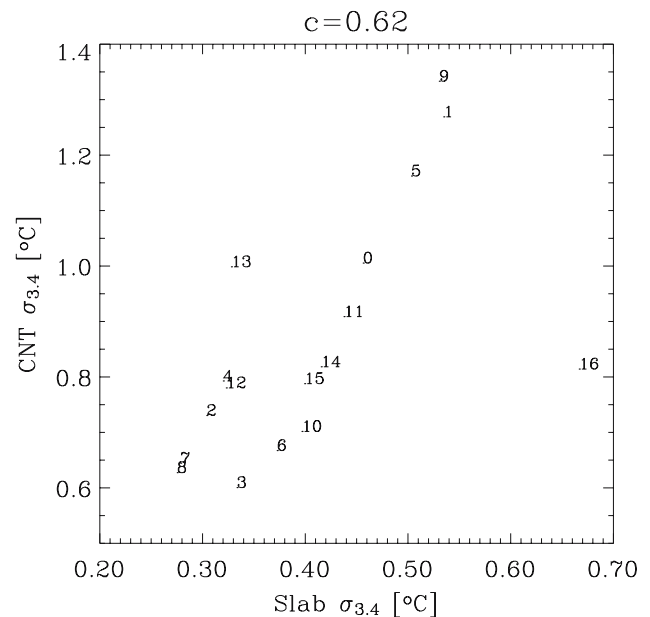


**Fig. 6** Correlation between equatorial SST variability in the NINO3.4 region of the coupled control ensemble (on the *y*-axis) and of the parallel slab-model ensemble (on the *x*-axis). The correlation value is given at the top of the plot

advected climatological near-surface vertical gradient of ocean temperature. Thus a wind stress anomaly pattern that is shifted further East results in greater anomalous SST tendencies and a stronger ENSO, consistently with Fig. 4.

#### 4 Intra-ensemble relationships between ENSO and mean climate

In order to compare the properties of the ENSO with those of the “background” climatology, we define an “ENSO-neutral” mean monthly and seasonal climatology by time-averaging quantities only over those years in which ENSO anomalies are not large. This is done by first defining an ENSO-neutral state as the NINO3.4 SST value at the peak of its frequency distribution (rather than its mean value) for each month. Subsequently, only a fraction, usually 0.5, of the available years is used, for which the mean-square NINO3.4 departure from its ENSO-neutral value is smallest. If this procedure is not used, the differences in the mean climatologies between ensemble members with very different ENSO variability carry an El-Niño type pattern that results from the positive skewness of the ENSO itself. (In particular, the reference SST climatology used for the flux-adjustment field is not recovered due to the rectification of the ENSO.)

We also analyse a suite of the parallel experiments of the (perturbed) atmosphere-only model coupled with a

static mixed-layer ocean (“slab” experiments) and also consider climatological properties of those. The exclusion of dynamical coupling with the ocean has implications for their mean state, which is corrected by a suitable flux-adjustment field for each member, but the differences between the climatologies of different members of the slab ensemble can be mainly attributed to the different behaviour of their atmospheric physics, while not being affected by the presence, as in the coupled case, of a coherent ENSO mode or dominant equatorial SST variability. They can thus help clarifying the effect of atmospheric parameter perturbations both for the model’s mean state, for the intrinsic variability of the atmosphere, and for their relationship with ENSO.

Figures 7, 8 and 9 all show cross-ensemble regressions (colour coding) and correlations (contour lines) of climatological fields with  $\sigma_{3,4}$ , the standard deviation (SD) of the NINO3.4 index of the coupled integrations (henceforth also called “control” ensemble, or “CTL”). There is a good agreement between maps derived from the ENSO-neutral control climatology and from the slab climatology. Large

and highly significant relationships are found between the strength of the ENSO and the heat and radiation fluxes of the background climatology. Within our ensemble, strong ENSO activity tends to occur in conditions of increased out-going “TOA” radiation fluxes. (The climate drift this would cause is neutralised by the surface-flux corrections applied.) Much of the TOA signal occurs in the oceanic subtropical bands (Fig. 7, upper panels), with a large area in the Southern Hemisphere. Particularly large increasing TOA flux occurs over the marine stratocumulus areas at the eastern sides of the subtropical anticyclones. Ocean-to-atmosphere heat fluxes (Fig. 7, lower panels) tend to compensate for the higher TOA radiation, as in part expected from flux-adjustment. In the CTLs an increase in the areas of the Western boundary currents is visible which is not as strong in the slab integrations; both cases however again show the strongest increases in the stratocumulus areas. Figure 8 highlights the contributions from TOA long-wave and surface short-wave radiation to the heat fluxes. Both control ENSO-neutral and slab-mean climatologies indicate radiative changes associated with low

**Fig. 7** Cross-ensemble regression (colour-coding) and correlation (contour lines) maps, of climatological fields against the NINO3.4 variability. In each case, the 17 fields of the ensemble members are regressed/correlated point-by-point with the corresponding 17 values of the NINO3.4 SD in CTL. The *left-hand side* maps are for the ENSO-neutral climatological fields of the CTL ensemble; the *right-hand side* maps are for the climatologies of the parallel slab ensemble. The *upper panels* show the regressions (correlations) of net upward “TOA” radiation; the *bottom panels* show regressions and correlations of the total net upward surface heat fluxes over ocean points. Contour lines are drawn at correlation values of  $-0.8$ ,  $-0.6$ ,  $0.6$  and  $0.8$ ; *solid lines* for positive correlations, *stippled lines* for negative correlations. Units for the regressions (colour coding) are  $\text{W m}^{-2} \text{ } ^\circ\text{C}^{-1}$

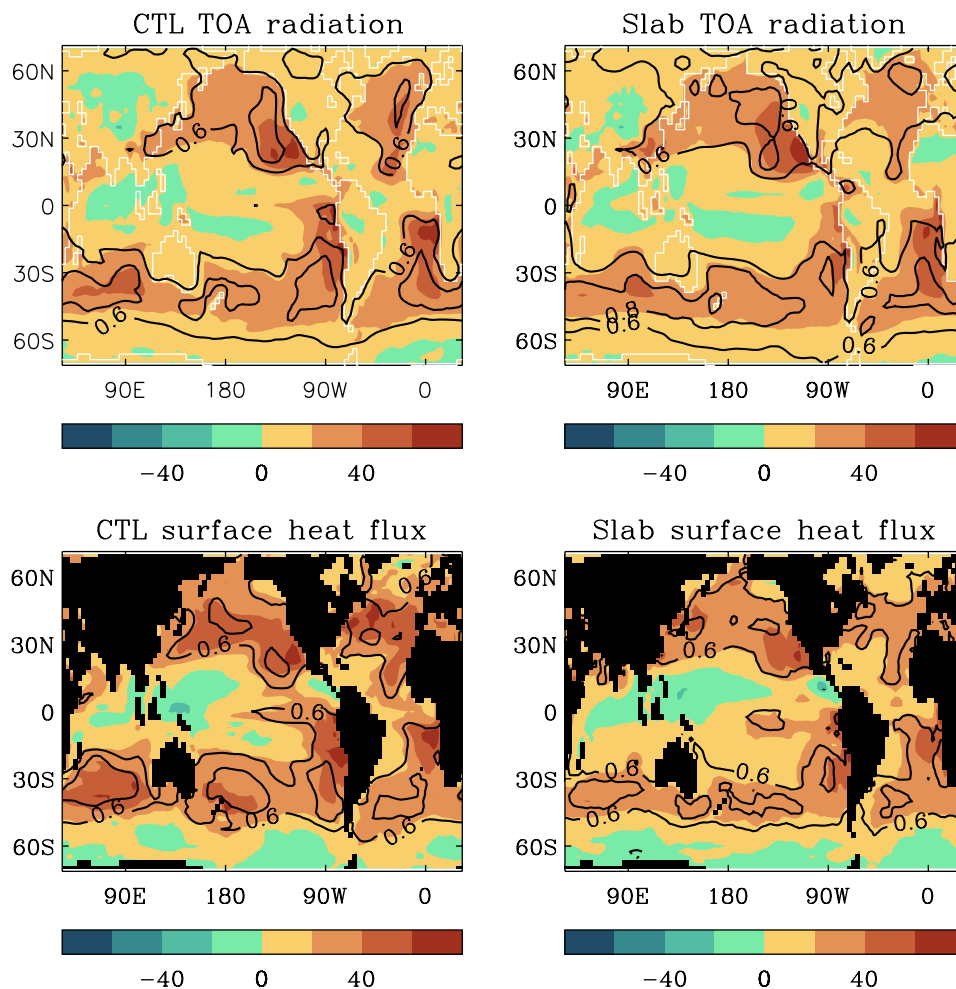
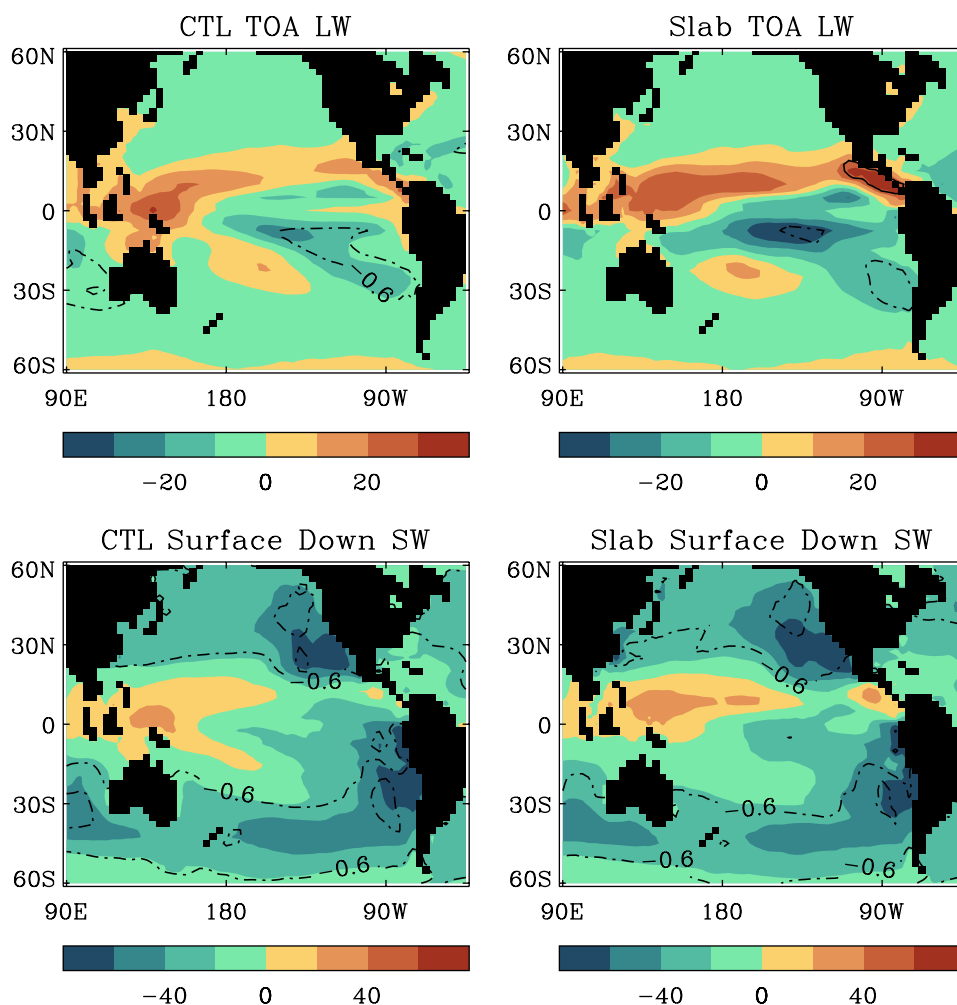


**Fig. 8** Similar to Fig. 7 but for the upward top-of-the-atmosphere long-wave radiation (panels on the top) and for the net downward surface short-wave radiation (panels on the bottom)



clouds over marine areas, with a strong surface SW component (negative downward) and a weaker TOA LW component. The latter however also indicates an hemispheric asymmetry with slightly reduced outgoing LW south of the Equator and slightly increased LW north of the Equator, suggesting a stronger cooling impact, reflected in TOA fluxes, of low-cloud cover in the North Pacific than in the south Pacific. This is confirmed by the net heating of the atmospheric column (upper panels of Fig. 9) showing a predominant diabatic warming of the atmosphere south of the Equator and a concomitant diabatic cooling North of the Equator in the Pacific sector in models with a stronger ENSO. The relation is more evident in the slab ensemble, while in the coupled ensemble ocean processes may be responsible for weakening the diabatic heating near the Equator and redistribute some of it northwards. In both the control and the slab ensembles, however, the atmosphere responds to the altered diabatic (mainly radiative) forcing with increased precipitation in the sub-equatorial central Pacific (Fig. 9, lower panels), at the eastern edge of the SPCZ, which drives a corresponding low-level circulation

anomaly (with respect to the ensemble mean) emanating from the intensified northern subtropical anticyclone and converging at the western edge of the southern anticyclone (which shows a much weaker intensification), with highly significant southward cross-equatorial component, and a weakened easterly component in the Southern Hemisphere.

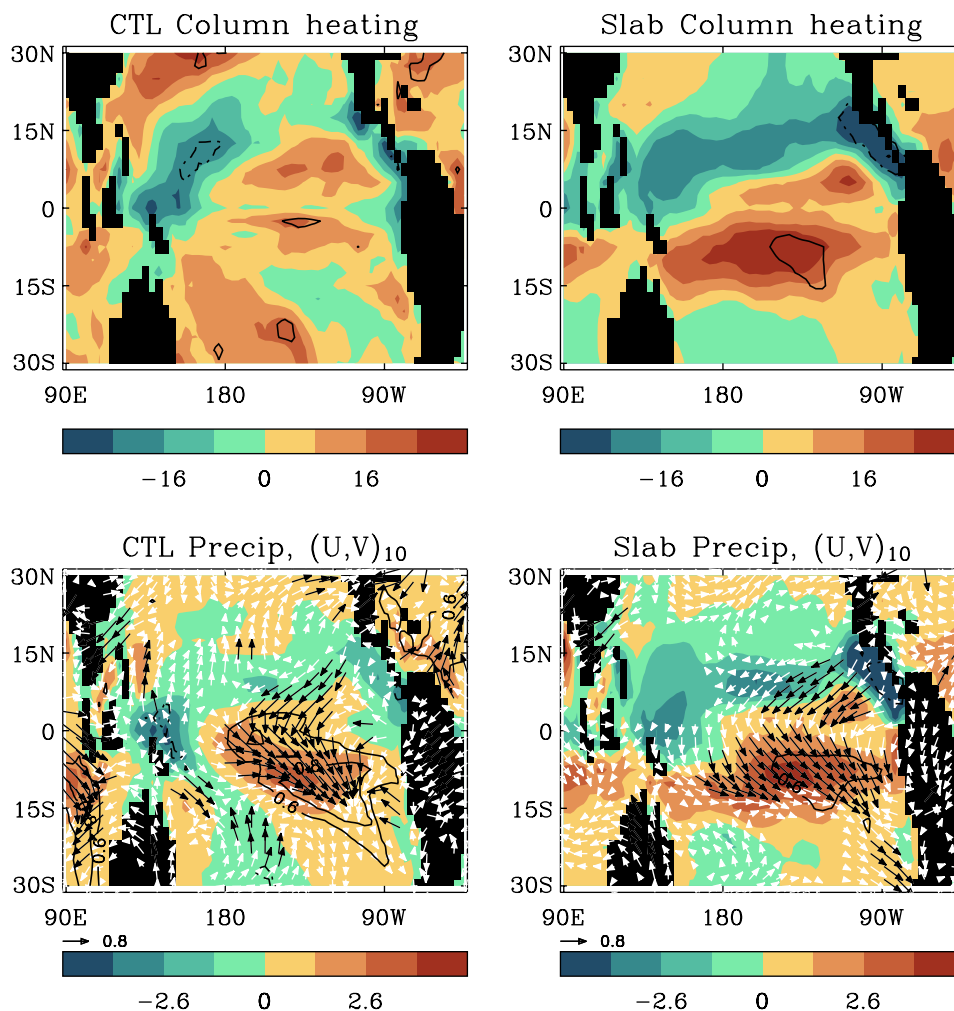
The control cross-ensemble correlations of NINO3.4 SD  $\sigma_{3.4}$  with the mean precipitation and the low-level convergence in the area 170W–110W, 15S–5S are 0.82 and 0.79, respectively; with the westerly surface wind between the same latitudes and 160E–150W it is 0.69. Similarly high correlation values are found with the slab climatologies, although geographically they are located slightly further south.

It is interesting to note that the correlations of the mean slab climatology with the SD of the slab NINO3.4 index are generally weaker than those of the same climatologies with  $\sigma_{3.4}$ .

The relationship between the SDs of  $\sigma_{3.4}$  and the strength of the seasonal cycle of the corresponding members (measured either by the SD of the mean ENSO-neutral cycle, or



**Fig. 9** Similar to Fig. 7 but for the net atmospheric-column heating (*panels on the top*) and for the total precipitation (*panels on the bottom, colours and contour lines*). The arrows in the bottom panels show the correlations of the 10-m winds with  $\sigma_{3,4}$  (arrows are drawn in black where the correlation exceeds 0.6). The units for the regression maps are  $\text{W m}^{-2} \text{ } ^\circ\text{C}^{-1}$  (*upper panels*) and  $\text{mm day}^{-1} \text{ } ^\circ\text{C}^{-1}$



by the total power in the 3- to 15-month frequency band of the full time-series; cf. Guilyardi 2006) are generally weak, and weaker than the relationship of each of these with the annual-mean climatology. In the tropical south Pacific, the annual means tends to be strongly related with the DJF and MAM mean climatologies. For example, weaker mean easterlies are associated with strong relaxation in MAM rather than with smaller wind-speeds in JJA; and similarly for the precipitation in the south-east tropical Pacific (SETP). However, the largest correlation values with  $\sigma_{3,4}$  are found with the monthly-climatological southern easterlies in August and with the south-east Pacific precipitation in September, during the growing stage of ENSO anomalies.

No correlation at all exists between the strength of the seasonal cycle on the Equator and  $\sigma_{3,4}$ . This conclusion may seem at odds with the results of Guilyardi (2006), but it may also be due at least in part to our use of monthly-mean flux-correction fields, which are initially computed using a relaxation time-scale of only about 15 days to the reference monthly climatology and have therefore a strong seasonal cycle themselves.

## 5 ENSO and atmospheric response to SST anomalies

From the previous sections we have learned that the differences in ENSO strength between different members of our perturbed-physics ensemble depend mainly on atmospheric processes, and in particular on changes in cloud cover that affect the mean heating and the background low-level circulation in the south Pacific. We now need to try and understand the physical link between these relations and the size of equatorial SST anomalies. In general, we expect the atmospheric response to changes in SSTs to be dependent on the background climatology of low-level wind convergence and vertical stability, which affects the local proneness to precipitating convection. The latter can determine the efficiency with which warm SST anomalies heat the atmosphere and drive changes in the surface winds that self-sustain the atmospheric anomalies themselves, and produce an ocean-atmosphere feedback loop via oceanic surface advection and upwelling.

We can diagnose a precipitation sensitivity in an ensemble member by computing the regression of local

precipitation anomalies to local SST anomalies, i.e. the quantity

$$\Pi = \left\langle \delta\text{PPT} \cdot \delta\text{SST} / \langle (\delta\text{SST})^2 \rangle \right\rangle, \quad (1)$$

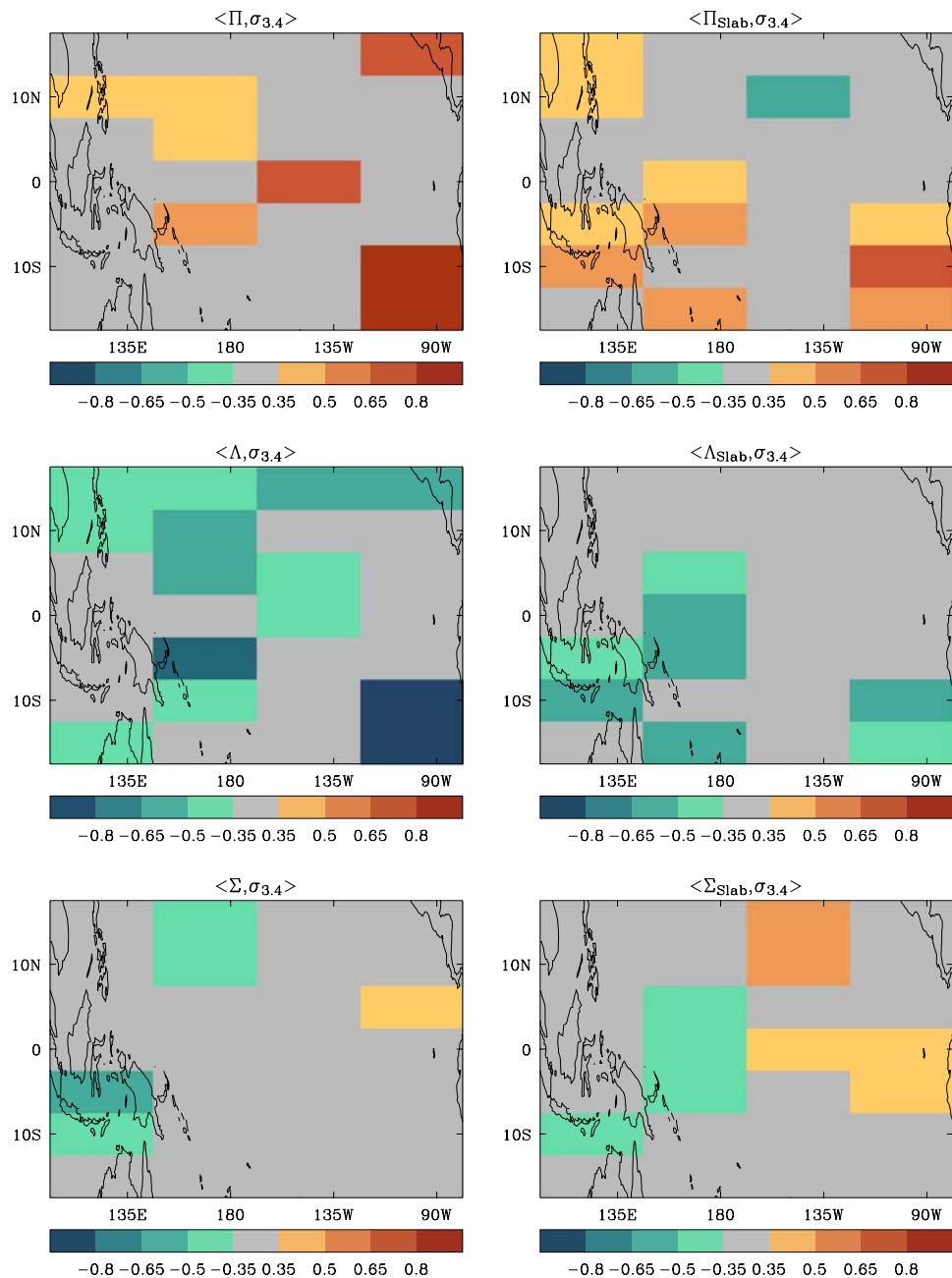
which expresses the change in precipitation per unit SST anomaly ( $\delta$  indicates deviation from the time-average). A larger value of  $\Pi$  in any member indicates a greater local precipitation anomaly for the same SST anomaly.

We similarly define regression fields for the TOA outgoing long-wave,  $\Lambda$ , and for the downward surface short-wave radiation,  $\Sigma$ , for each of the members of the coupled CTL and of the slab ensembles. For the former, to avoid

contamination by the (non-local) ENSO signal itself, we apply our procedure to define ENSO-neutral conditions and consider only the 20 years, out of 80, with the nearest ENSO-neutral state. The model data was averaged over  $45^\circ \times 5^\circ$  boxes (corresponding to  $12 \times 2$  grid-points) before the regression fields  $\Pi$ ,  $\Lambda$  and  $\Sigma$  were calculated, and Fig. 10 shows the correlation maps of such regression fields with  $\sigma_{3,4}$ . Again there is reasonable consistency between the correlations obtained from the CTL and the slab integrations.

Ensemble members with a stronger ENSO tend to have larger precipitation sensitivity  $\Pi$  (top panels), particularly in the SETP near the south American coast. This is

**Fig. 10** Cross-ensemble correlations of  $\sigma_{3,4}$  with  $\Pi$  (Eq. 1) the local precipitation regression onto local SST anomalies (top panels), and with  $\Lambda$  (panels in the middle) and  $\Sigma$  (bottom panels), the local outgoing TOA long-wave and downward surface short-wave regressions, respectively. The model data was spatially binned before computing the regressions



accompanied with more strongly reduced outgoing long-wave radiation when SSTs are locally raised (middle panels), while the surface short-wave signal is weak, suggesting no strong correlation with cloud-cover response but rather with cloud-top altitude. There is in fact even a hint that the SW signal is positive in the East Pacific, consistent with the suggestions that layer clouds can be more easily replaced with cumulus in members where ENSO is strong.

The region with the highest correlation between  $\Pi$  and  $\sigma_{3.4}$ , comprised within the area 17.5S–7.5S, 125W–80W (which we shall henceforth refer to as south-east tropical Pacific area, or “SETP”) is itself affected by ENSO in the coupled models, and tends to experience positive SST anomalies when NINO3.4 is positive. By filtering out ENSO years however we have removed that signal, and we have verified that the SST anomalies over the SETP region during ENSO-neutral years, as found by our definition, do not correlate significantly with NINO3.4 at any lag (correlations values are smaller than 0.20). Using ENSO-neutral years we can therefore isolate the contribution to atmospheric anomalies of SETP SST anomalies.

Figure 11 shows the mean across each ensemble (CTL and Slab) of the anomalies associated with its own SETP variability. They essentially represent a relative weakening of the southern subtropical anticyclone and of ITCZ-convection in the area of the Gulf of Panama, with associated cross-equatorial northerly low-level flow and also a positive zonal component spreading from Southern Hemisphere onto the Equator. Thus, the periodical warming of the southern stratocumulus area can lead to reduced equatorial upwelling in the central Pacific. This may lead us to expect that there should be a correlation between SETP variability and ENSO variability, as is indeed seen in Fig. 12. The effect on equatorial variability can be directly gauged from

the differences between the correlations between the SD of SETP variability and the regressions of SST, precipitation and wind anomaly fields on SETP itself across the two ensembles. Figure 13 shows that, as SETP variability gets stronger, anomalies on the Equator are increasingly affected in the CTLs, with warm SST, westerly wind and positive precipitation anomaly appearing. But, in spite of all other previously noted similarities, this behaviour is not apparent in the Slab integrations (Fig. 13), where in fact equatorial precipitation seems to enter in competition with increased activity in the Southern Hemisphere.

### 6 Summary

We have examined the ENSO behaviour in a 17-member ensemble of the HadCM3 model in which perturbations are made to parameters in the atmospheric component of the model. Despite the identical ocean components in each member, the imposition of flux adjustments which render the mean surface climatologies near-identical, and the common model structure, there is a wide range of ENSO characteristics across the ensemble (Fig. 1). Related variations are seen in both amplitude, frequency and centre-of-action of the ENSO variability (Figs. 2, 4), and those variations are comparable to those seen in the multi-model ensembles (e.g. van Oldeborgh et al. 2006).

In this ensemble, the equatorial thermocline feedback does not appear to be very strong and cannot explain intra-ensemble variations in ENSO characteristics. Ensemble members with a stronger ENSO generally display an increased tendency for westward propagation of the SST anomalies (Fig. 5), which are thus recognisable as surface (or “SST”) modes mainly dependent on anomalies

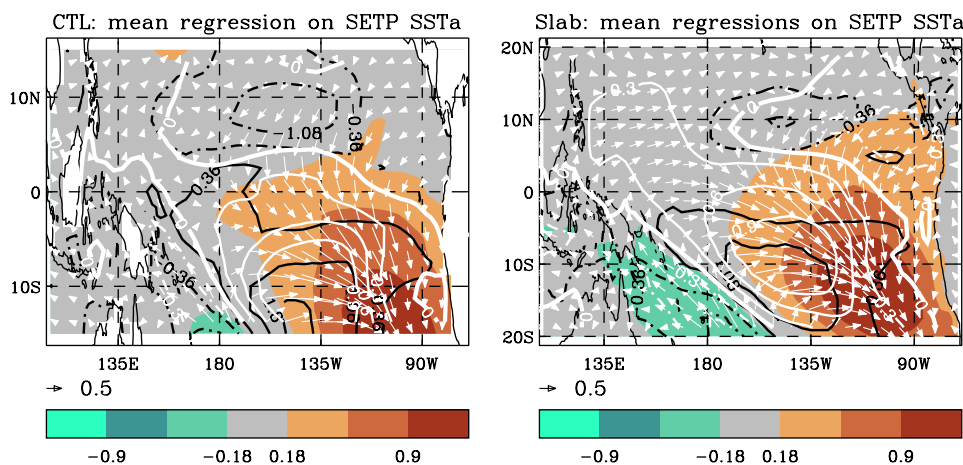
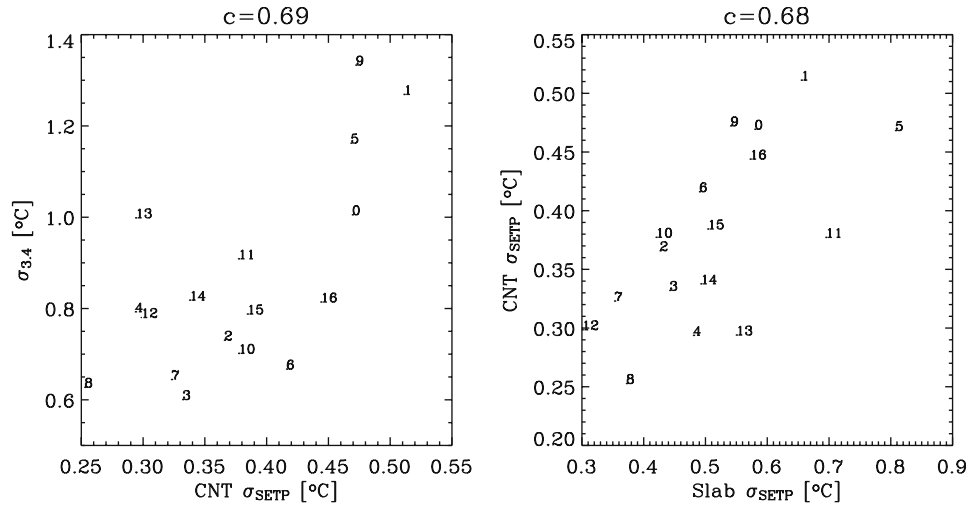


**Fig. 11** Ensemble means of the regression fields of SSTs (colours), precipitation (black contour lines) and 10-m winds (arrow symbols for the velocity vectors and white contour lines for the zonal component)

onto SETP SST anomalies. The left-hand-side panel refers to the coupled CTL ensemble and the right-hand side to the slab ensemble

**Fig. 12** Correlations between SETP variability and  $\sigma_{3,4}$



generated at or near the ocean surface. This is further supported by the relatively close relationship between equatorial SST variability in the coupled, or control, ensemble, and the parallel slab-ocean ensemble where ocean dynamics is entirely absent (Fig. 6). The strength of the ENSO may be therefore primarily controlled by the strength of surface-flux damping, and by the longitudinal location of the associated zonal wind anomalies (Fig. 4), which are more effective in producing anomalous SST tendencies from ocean surface advection and upwelling if centred on or east of the dateline, where the climatological zonal SST gradient is larger and the subsurface ocean is cooler. Surface-flux damping probably plays a role, as the SST variability in the slab integrations is reduced in members with a more negative regression of TOA

anomalies onto SST anomalies. The greatest sensitivity however is not located over the Equator. The strength of the ENSO is associated to variations in the properties of the mean climatology as determined by perturbed physical parameterisations (Figs. 7, 8, 9). We have shown that changes in the mean properties of climatological cloud cover, and especially an increase in low-level clouds, can lead to an increased proneness of the south-Pacific marine stratocumulus area to convective activity (Fig. 10). The associated relative weakening of the southern subtropical anticyclone calls forth northwesterly wind anomalies on and south of the Equator in the central-eastern Pacific (Fig. 11). Events of this kind are associated with increased SST variability in the south-east Tropical Pacific (SETP) area which directly correlates with ENSO activity (Fig.

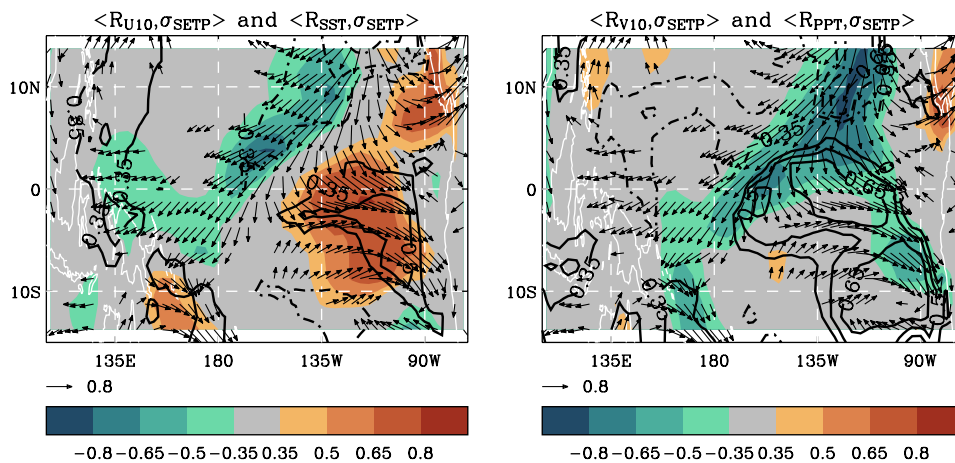


**Fig. 13** Cross-ensemble correlations of ENSO-neutral regressions onto SETP SST anomalies (see Fig. 11) with the SD of SETP anomalies for the CTL ensemble. As in Fig. 11, the regressions are for SSTs (contour lines, left-hand-side panel), precipitation (contour lines, right-hand-side panel), and 10-m winds (arrows and colours).

The colours in the left-hand-side panel refer to the zonal wind component, those in the right-hand-side panel to the meridional wind component. Negative correlations have blue tints or stippled contour lines. Arrows are only plotted for point with correlations larger than 0.5

**Fig. 14** Correlations of regressions onto SETP SST anomalies with  $\sigma_{3,4}$  for the Slab ensemble. Same as Fig. 13 but for fields from the Slab ensemble

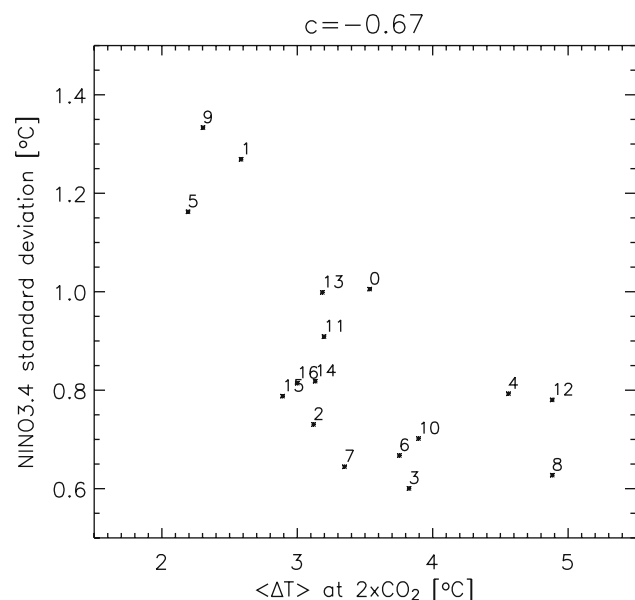
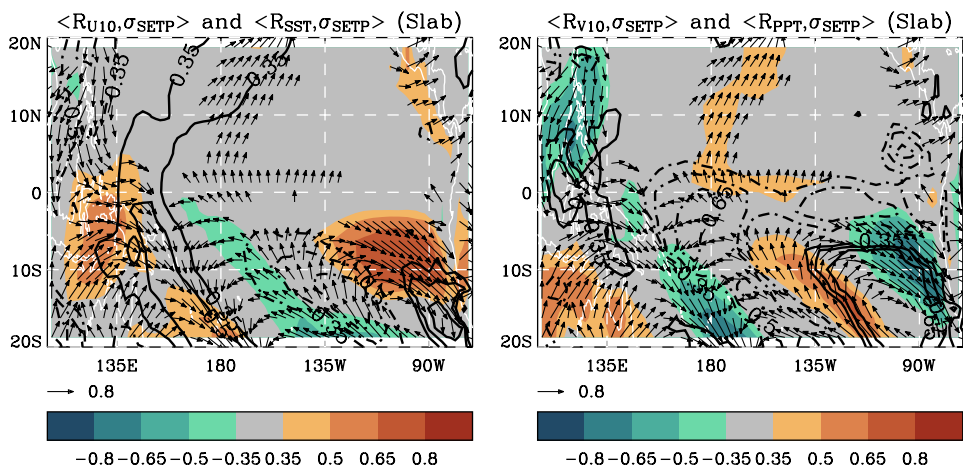


**Fig. 15** Climate sensitivity (defined as the global mean temperature change for a doubling of  $CO_2$ ) against ENSO amplitude (defined as the SD of NINO3.4 anomalies) across the perturbed physics ensemble

12). In both slab and coupled models, increased SETP activity is associated with increased SST variability over the Equator, but more so in the coupled models where, in addition to the wind-evaporation feedback, upwelling and advection can further promote growth (Figs. 13, 14).

### 7 Discussion and conclusions

In the perturbed-physics ensemble of the flux-adjusted HadCM3 model studied here, we have found that ENSO activity is promoted by localised SST variability in the SETP region, which is associated with alterations of the climatology associated with increased climatological

low-cloud cover. We further note a link between ENSO properties and climate-mean response to greenhouse forcing (Fig. 15). The amplitude of ENSO (and, by Fig. 2, its frequency and its centre-of-action) is negatively correlated with the climate sensitivity of the corresponding ensemble member. From the results of our analysis, identifying cloud cover as a significant contributing factor to the cross-ensemble spread in ENSO characteristics, this is consistent with the established importance of cloud-feedbacks in driving uncertainty in climate sensitivity in perturbed physics ensembles (e.g. Webb et al. 2006). This result might also support the view that cloud feedbacks operating during an ENSO event can provide a constraint on global-mean climate feedbacks (e.g. Bony and Dufresne 2005).

The increased facility to initiate convection in the SETP in the presence of more marine stratus cloud may seem paradoxical. One interpretation for this behaviour of the model is the effect of flux adjustment, which tends to compensate for an exceedingly negative heat budget in the atmospheric column by warming the surface. A second possible suggestion however is that the inter-hemispherically asymmetric response favours convection in the south-east Pacific as relatively stronger SW cooling is preferentially associated with a suppression of convection in the Eastern ITCZ north of the Equator, particularly the Gulf of Panama (Fig. 9). Suppressed precipitation in the ITCZ is found at a significant level in the JJA and SON seasons for integrations with strong cloud forcing.

Flux-adjustment has been found to actually affect the ENSO in HadCM3, reinforcing its tendency to be governed by a surface mode (or “SST” mode; Jin and Neelin 1993), probably in association with the formation of a sharp zonal gradient in the depth of the equatorial thermocline and the resulting degradation of the numerical representation of propagating baroclinic Kelvin waves, thus reducing the oceanic feedback involved in the thermocline mode (Spencer et al. 2007). However, while the dominance of



perturbations to atmospheric processes is related to the prevalence for SST-mode-like variability in all members, even in the presence of stronger ocean thermocline feedbacks the atmospheric loop of the ENSO feedback cycle would be likely to be regulated by perturbations to physical atmospheric processes. Our results are broadly consistent with the results from the HadCM3 equilibrium integrations (Toniazzo 2005, 2006), where it was shown that similar qualitative changes in the mean patterns of climatological convection in the tropical Pacific are concomitant with similar changes in the properties of the ENSO, with a predominant surface-mode response. More generally, this study reiterates the findings of Guilyardi et al. (2004) regarding the importance of the atmospheric component of a coupled AOGCM in determining ENSO characteristics. In the context of coupled model development, the implication is that ENSO characteristics may be very sensitive to the atmospheric parameters which are often used to “tune-out” radiative imbalances.

**Acknowledgments** The authors wish to thank Ben Booth and Glen Harris for their help in making the ensemble data available to us. The model integrations were performed at the Hadley Centre by the QUMP team. This work was supported by the UK Department of the Environment, Food and Rural Affairs under Contract PECD 7/12/37, by the Government Meteorological Research Contract, by the National Centre for Atmospheric Sciences (NCAS-Climate), and by the EU DYNAMITE project (contract 003903-GOCE).

## References

- AchutaRao K, Sperber KR (2006) ENSO simulation in coupled ocean–atmosphere models: are the current models better? *Clim Dyn* 27:1–15
- Bony S, Dufresne J-L (2005) Marine boundary layer clouds at the heart of tropical cloud feedback uncertainties in climate models. *Geophys Res Lett* 32:L20806. doi:[10.1029/2005GL023851](https://doi.org/10.1029/2005GL023851)
- Brown J, Collins M, Tudhope AW, Toniazzo T (2007) Modelling mid-Holocene tropical climate and ENSO variability: towards constraining predictions of future change with palaeo-data, 2007. *Clim Dyn*. doi:[10.1007/s00382-007-0270-9](https://doi.org/10.1007/s00382-007-0270-9)
- Capotondi A, Wittenberg A, Masina S (2005) Spatial and temporal structure of Tropical Pacific interannual variability in 20th century coupled simulations. *Ocean Model* 15:274–298
- Coelho CAS, Stephenson DB, Doblas-Reyes FJ, Balmaseda M (2006) The skill of empirical and combined/calibrated coupled multi-model South American seasonal predictions during ENSO. *Adv Geosci* 6:51–55
- Collins M, Tett SFB, Cooper C (2001) The internal climate variability of HadCM3, a version of the Hadley Centre coupled model without flux adjustments. *Clim Dyn* 17:61–81
- Collins M, Booth BBB, Harris GR, Murphy JM, Sexton DMH, Webb MJ (2006a) Towards quantifying uncertainty in transient climate change. *Clim Dyn* 27:127–147
- Collins M, Bhaskaran B, Booth B, Harris G, Murphy J, Sexton D, Webb M, Brierley C (2006b) Progress and plans for probabilistic climate prediction at the Hadley Centre. *Geophys Res Abstracts*, vol 8, 05738, 2006
- Gordon C, Cooper C, Senior CA, Banks H, Gregory JM, Johns TC, Mitchell JFB, Wood RA (2000) The simulation of SST, sea ice extents and ocean heat transport in a version of the Hadley Centre coupled model without flux adjustments. *Clim Dyn* 16:147–168
- Guilyardi E (2006) El Niño-mean state-seasonal cycle interactions in a multi-model ensemble. *Clim Dyn* 26:329–348
- Guilyardi E, Gualdi S, Slingo J, Navarra A, Delecluse P, Cole J, Madec G, Roberts M, Latif M, Terray L (2004) Representing El Niño in coupled ocean-atmosphere GCMs: the dominant role of the atmospheric component. *J Clim* 17:4623–4629
- Jin F-F, Neelin JD (1993) Modes of interannual tropical ocean–atmosphere interaction—a unified view, III, Analytical results in fully coupled cases. *J Atmos Sci* 50:3523–3540
- Johns TC, Carnell RE, Crossley JF, Gregory JM, Mitchell JFB, Senior CA, Tett SFB, Wood RA (1997) The second Hadley Centre coupled ocean-atmosphere GCM: model description, spin-up and validation. *Clim Dyn* 13:103–134
- Joseph R, Nigam S (2006) ENSO evolution and teleconnections in IPCC’s twentieth-century climate simulations: realistic representation? *J Clim* 19:4360–4377
- Merryfield WJ (2006) Changes to ENSO under CO<sub>2</sub> doubling in a multi-model ensemble. *J Clim* 19:4009–4027
- Murphy JM, Sexton DMH, Barnett DN, Jones GS, Webb MJ, Collins M, Stainforth DJ (2004) Quantification of modelling uncertainties in a large ensemble of climate change simulations. *Nature* 430:768–772
- Philip SY, van Oldenborgh GJ (2006) Shifts in ENSO coupling processes under global warming. *Geophys Res Lett* 33:L11704. doi:[10.1029/2006GL026196](https://doi.org/10.1029/2006GL026196)
- Rayner NA et al (2003) Global analyses of sea surface temperature, sea ice, and night marine air temperature since the late nineteenth century. *J Geophys Res* 108 doi:[10.1029/2002JD002670](https://doi.org/10.1029/2002JD002670)
- Spencer H, Sutton R, Slingo JM (2007) El Niño in a coupled climate model: sensitivity to changes in mean state induced by heat flux and wind stress corrections. *J Clim* 20:2273–2298
- Toniazzo T (2005) A study of the sensitivity of ENSO to the mean climate. *Adv Geosci* 6:111–118
- Toniazzo T (2006) Properties of El Niño Southern Oscillation in different equilibrium climates with HadCM3. *J Clim* 19:4854–4876
- van Oldeborgh GJ, Philip SY, Collins M (2005) El Niño in a changing climate: a multi-model study. *Ocean Sci* 1:81–95
- Webb MJ, Senior CA, Sexton DMH, Ingram WJ, Williams KD, Ringer MA, McAvaney BJ, Colman R, Soden BJ, Gudgel R, Knutson T, Emori S, Ogura T, Tsushima Y, Andronova N, Li B, Musat I, Bony S, Taylor KE (2006) On the contribution of local feedback mechanisms to the range of climate sensitivity in two GCM ensembles. *Clim Dyn* 27:17–38